Environmental Engineering and Management Journal

May 2020, Vol.19, No. 5, 721-731
http://www.eemj.icpm.tuiasi.ro/; http://www.eemj.eu

"Gheorghe Asachi" Technical University of Iasi, Romania

DECONTAMINATION OF PESTICIDE RESIDUES IN WATER SAMPLES USING COPPER AND ZINC CO-DOPED TITANIA NANOCATALYST

Tentu Nageswara Rao[1*], Pulapalli Babji[2], Botsa Parvatamma[3], Tentu Manohra Naidu[4]

[1]School of Materials Science and Engineering, Changwon National University, Changwon, Gyeongnam, 641-773, Republic of Korea
[2]Department of Physical, Nuclear Chemistry & Chemical Oceanography, School of Chemistry, Andhra University, Visakhapatnam Andhra Pradesh, India
[3]Department of organic Chemistry, Gayathri P.G Courses, Gotlam, Vizianagaram, AP, India
[4]Department of nuclear physics, Andhra University, Visakhapatnam, Andhra Pradesh, India

Abstract

Copper and Zinc co-doped titania nano photocatalyst (Cu-Zn-TiO_2 NPC) was fabricated and characterized using room temperature X-ray diffraction (XRD), field emission electron microscopy (FESEM) with high-resolution transmission electron microscopy (HRTEM) and energy dispersion X-ray (EDX). X-ray diffraction studies of the Cu^{2+}-Zn^{2+}/TiO_2 show the presence of anatase phase TiO_2 and in the sample prepared from 0.05, 0.10, 0.15 and 0.20 mmol have also shown the presence of anatase phase only. The photocatalytic efficiency of the synthesized catalysts was investigated by the photocatalytic degradation of aqueous bispyribac sodium under sun light irradiation, and it was found that the Cu and Zn co-doped TiO_2 catalysts has better photocatalytic activity. It can be also showed that with the addition of dopants to titania hinders the growth of nanoparticles. This can be attributed of the fact that there is a more efficient electron-hole creation in Cu and Zn co-doped TiO_2 in sunlight, contrary to un-doped TiO_2 which can be excited only in UV irradiation. Photocatalytic studies of bispyribac sodium at various conditions such as acidic, basic and neutral reveals that the activity is enormously increased with co-doped TiO_2 is proved to be effective for photocatalysis of bispyribac sodium and is more effective in basic medium.

Keywords: bispyribac sodium**,** Cu-Zn-TiO_2 NPC, DT 50, FTIR, photocatalytic activity, XRD

Received: June, 2019; Revised final: October, 2019; Accepted: November, 2019; Published in final edited form: May, 2020

1. Introduction

Pesticides enter natural water bodies by direct application and leaching from the soil and vegetation. Many of these chemical compounds in aqueous media can undergo sunlight photochemical transformation via direct or indirect photoreaction. Among several agents of the environment, sunlight visible and ultra-violet is the most powerful to degrade the environmental contaminants like pesticide residues. Photocatalysis is being commonly used in industry for the effective decontamination of large quantities of effluents and other wastages to protect the environment and human health. Semiconductor photocatalysis has emerged recently as a promising technology to decontaminate the environment. Titanium dioxide among other semiconductors has been under immense investigation for practical applications such as in antimicrobials, air and water purification (Byrne et al., 2019; Impellizzeri et al., 2016) deodorization, and wastewater treatment of reasons such as their favorable physicochemical properties (Geraldine et al., 2018), low cost, easy accessibility and high stability (Fujishima et al., 2000; Rehman et al., 2009). However, it is active only under UV irradiation (λ=388 nm), which accounts for less than 5% of solar light (Amoros-Perez et al., 2019; Mahy et al., 2018; Pelaez et al., 2012). As a result of

* Author to whom all correspondence should be addressed: e-mail: tnraochemistry@gmail.com

vast research various attempts were made to utilize visible light with TiO_2 photocatalysis, including dye sensitization, semi-conductor coupling and impurity doping (Kim and Choi, 2005; Li and Li, 2001; Moon et al., 2003). Co-doped TiO_2 has been shown to exhibit smaller particle sizes and higher surface area that significantly increases its activity with other reagents (Asahi et al., 2001; Choi et al., 1994). Depositing noble metal nanoparticles (Dawson and Kamat, 2001) and coupling with secondary semiconductors (Ge et al., 2006).

Co-doping titania with a few transition metals and some non-metal ions has been reported (Asahi et al., 2001; Choi et al., 1994; Li et al., 2003). Few data are available on co-doping the nano-catalyst TiO_2 with Cu (II) and Zn (II) metal ions (Mohamed et al., 2018; Tobaldia et al., 2016; Zhang et al., 2018). Keeping that in view, an attempt was made here to synthesize Cu-Zn co-doped TiO_2 nano-catalyst by sol-gel method and investigate its photo-catalytic performance by specifically using the bispyribac sodium (Fig. 1) herbicide under visible light at different experimental conditions.

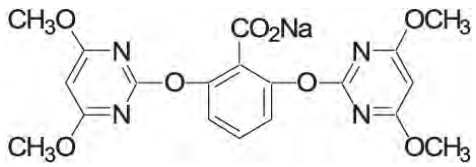

Fig. 1. Chemical structure of Bispyribac sodium

2. Material and methods

2.1. Chemicals and reagents

Titanium tetra-n-butoxide [$Ti(O\text{-}Bu)_4$], Potassium dihydrogen phosphate (KH_2PO_4), disodium hydrogen orthophosphate (Na_2HPO_4), boric acid (H_3BO_3), potassium chloride (KCl), formic acid (HCOOH), acetonitrile (ACN) and sodium hydroxide (NaOH), Humic Acid, surfactants cetyltrimethylammoniumbromide (CTAB), sodium dodecyl sulfate (SDS) and Brij-35 obtained from Analytical grade of Merck (Germany) was used as titanium, Copper Nitrate and Zinc Acetate sources for preparing Cu^{2+} and Zn^{2+} co-doped TiO_2 photocatalysts and bispyribac sodium (purity 99.8%), reference analytical standard was pursed from Sigma-Aldrich (USA). HPLC grade Acetonitrile and GR grade orthophosphoric acid was taken from the Merck India limited. We used the Milli-Q Plus device (Millipore, Bedford, MA, USA) to purify distilled water. Super dry purified ethyl alcohol from Changshu Yangyuan Chemical, China has been used.

2.2. Preparation of Cu-Zn-TiO_2 NPs

Tetrabutyl orthotitanate (0.02 mol) was added drop by drop in 50 ml of ethyl alcohol (98.79%) and stirred gently for 20 minutes at room temperature. Three drops of concentrated HNO_3 has been added to the solution.

The desired amounts ($0.05 \leq x \leq 0.20$ mmol) of copper nitrate and zinc acetate (the molar ratio of Cu to Zn was 1:1) were used in the reaction mixture while continuously stirring for 60 min until dissolving of Cu and Zn dopants. In the same solution, 2 mL of distilled water has been added. The solution was maintained at room temperature with constant stirring for 2 h to achieve a gel that was agitated at room temperature for 12 hours. The gel was dried overnight at 80±2°C and annealed for 3 hours at 400 °C. The resulting material appeared light gray in color. By adopting the above procedure, a pure TiO_2 composition was also synthesized that was used for comparison purpose.

2.3. Characterization

The sample morphology and chemical composition were explored using FESEM (FEI, Quanta 200) and EDX (EDX, connected to the SEM) respectively. Identified the crystal structure using XRD analysis performed at a scan rate (2 θ) of 15° min^{-1} ranging from 5° to 70°. FT-IR spectra for Cu^{2+} and Zn^{2+} the IR-Prestige-21 Shimadzu FT-IR spectrophotometer was obtained from KBr pellet method in the range 4,000 to 400 cm^{-1}. HRTEM (FEI, TECNAI G2 TF20-ST) Assessed particle size with a 200 kV acceleration voltage. The UV-Vis diffuse reflectance spectra (DRS) was mapped on a spectrophotometer (Shimadzu UV-3600).

2.4. Preparation of acidic, neutral and basic water

The 8 g of KH_2PO_4 has been dissolved in 1000 ml distilled water for acidic water preparation. The pH of the buffer was changed in accordance with 4.0 with the same. For preparing the neutral water 6.3 g of Na_2HPO_4 and 5 g KH_2PO_4 has been dissolved in 1 000 ml of double distilled water. The pH of the buffer was changed in accordance with 7.0 with the same. On the other hand, basic water as prepared by dissolving the 12.5 g of H_3BO_3 and 15 g KCl in 1000 ml of distilled water. The pH was adjusted to 9.0 using 0.1M NaOH solution.

2.5. Preparation of bispyribac sodium sample stock solution

Accurately 98.82 mg of sample (purity 10.12%) of bispyribac sodium was taken in a 20 ml volumetric flask; 5 ml of acetonitrile is added in a same volumetric flask, sonicated and made sufficient with the acetonitrile. The solution concentration achieved 500 mg / L. This solution of the stock sample was utilized for the preparation of dose samples in distinct aqueous solutions.

2.6. Instrumental conditions for quantifying bispyribac sodium

The residue was quantified using Shimadzu HPLC LC-20AT quaternary pump high-pressure Liquid Chromatography with diode photo array detector. The detector wavelength was set at 245 nm.

The separation of bispyribac sodium was carried out using the Zorbax® column SB-octadecyl (particle size (5 µm), diameter (4.6 mm) and length (150 mm)). The mobile phase was used (ACN: 0.1% HCOOH, 55:45, v / v) and the oven temperature was kept at 30 ° C. The flow rate of 1,0 ml per minute was set. The flow of 1.0 ml per minute flow rate was set. The injection volume 20 µl was set for standard and sample. The bispyribac sodium was eluted at 3.8 minutes. Unchanged residues of bispyribac sodium were confirmed by re-analyzing the representative samples using a High Capacity Ion Trap LC-MS/MS System of Bruker Daltonik GmbH. Drying gas nitrogen was generated from the atmospheric air in a Nitrox UHPLCMS nitrogen generator. The nebulizer gas nitrogen flow was fixed to 10 L/min. MS / MS mode operation was performed with helium as collision gas at 4 x 10-4 millibar pressure. In positive ionization mode, a capillary voltage of 3.5 kV was used. The interface temperature was set at 360 °C. The scan range was 50 - 460 m/Z. Agilent 1200 HPLC system with Zorbax® column SB-C18 (particle size (3.5 µm), diameter (4.6 mm) and length (75 mm)), gradient program with 0.4 ml per minute flow rate having 0.1% HCOOH in ACN as mobile phase A and 0.1% HCOOH in HPLC grade water as mobile phase B was used. For mobile phase A, the flow program was used from 5% to 95%.

2.7. Adsorption study of the catalyst

Recovery studies in water and different pH waters were conducted with 0.1 g L^{-1} level of catalyst and reported % of recoveries in distilled water and different pH water.

2.8. Limits of Quantification (LOQ)

The LOQ (mg/L) has been determined as the lowest analyte concentration giving a response often times the baseline noise.

2.9. Photolytic and photocatalytic study

The photocatalysis of bispyribac sodium in water was studied by spiking bispyribac sodium 10% SC formulation at 1 mg L^{-1}. The study was conducted in different pH waters at 0.1 mg/L (a.i) fortification level. We prepared 2 sets; one set was used for photolytic study (Without added photo catalyst) and second set of samples were added Cu-Zn-TiO_2 NPs to get 0.1 g L^{-1} content of photocatalyst (optimum amount). The sample suspensions of Cu-Zn-TiO_2 NPs were sonicated in the dark for 10 min before exposure to the sunlight, to get even disperses of Cu-Zn-TiO_2 NPs in water and attain adsorption equilibrium. The samples were exposed to direct sunlight. Aliquots of samples (4 replications) were collected on pre-determined intervals. The temperature of water samples during the period was 25 to 42°C. The samples collected on various sampling occasions and were filtered using a 0.2 µm PTFE membrane filter and collected in amber-colored vials. All the samples were stored in dark at <5°C before subjecting to HPLC-DAD analysis. The samples fortified with Cu-Zn-TiO_2 NPC particles were centrifuged using Beckman cooling centrifuge at 10000 rotations per minute for 4 minutes at 5°C. Transferred the supernet into the amber colored bottles and stored in dark at<5°C until analysis to avoid further degradation of residues.

2.10. Effect of surfactants on water decontamination

To study the impact of surfactants on pesticide decontamination in water, water was spiked with 1mL of 100 mg/L stock solution of bispyribac sodium formulation to get 0.1µg/mL concentration of pesticide active in water (each pesticide was spiked into separate one litre glass bottle) and loaded with 0.1 g L^{-1} Cu-Zn-TiO_2 NPC (optimum amount) were added with 10^{-2} mole/L concentration of cationic surfactants CTAB, anionic surfactant SDS and nonionic surfactant Brij-35.

The samples were sonicated in the dark for 10 minutes before exposure to the sunlight, to get even disperse of Cu-Zn-TiO_2 NPC in water and attain adsorption equilibrium. The samples were exposed to sun light in the month of June.

2.11. Effect of humic acid content

To study the impact of humic acid content on pesticide decontamination in water, water was spiked with 1 mL of 100 mg/L stock solution of bispyribac sodium formulation to get 0.1µg/mL concentration of pesticide active in water, added optimum amount of catalyst and added humic acid (Prepared by 100 mg of humic acid dissolved in 0.1 M NaOH solution and diluted with 1000 mL of distilled water) by varying the concentration of 0, 10 and 20 mg/L in water. The samples were sonicated in the dark for 10 min before exposure to the sunlight, to get even disperse of Cu-Zn-TiO_2 NPC in water and attain adsorption equilibrium. The samples were exposed to sun light in the month of June.

3. Results and discussion

3.1. XRD Study

Fig. 2 shows the XRD profiles of the pure as well as the co-doped TiO_2 powders. Crystals in the anatase phase were confirmed in all the samples (Gao et al., 2006). No diffraction peak corresponding to Cu and Zn were detected. The reason might either be that the content of Cu and Zn is too low or they are too well-dispersed in the TiO_2 particles. The diffraction patterns of the doped Cu-Zn-TiO_2 NPC samples are identical to that of the un-doped TiO_2. The inset in Fig. 2 displays intensified crystal plane XRD peaks (101) for all samples. Compared with pure TiO_2, peak shift is observed in the doped samples. An increase in the intensity of the pure anatase TiO_2 sample was observed with the increasing doping and the peaks corresponding to copper nitrate and Zinc acetate were

not detected. The patterns of the XRD match the JCPDS number: 21-1272.

Two factors mainly determine the doping mode: electronegativity and the dopants ' ionic radius. If the electronegativity and the ionic radius of the doping ions match those of the oxide lattice ions, the doping ions may replace the lattice ions during the doping process (Cao et al., 2004).

The lattice parameters and crystal sizes of the samples were calculated using the diffraction peaks and the values were presented in Table 1. It is found that the amount of cell volume of Cu-Zn-TiO_2 NPC has been larger than that of un-doped TiO_2.

Because Zn and Cu metals are incorporated into the TiO_2 matrix, the reduction in the particle size of TiO_2 could be attributed to an extending effect. Reducing the intensity and widening the reflection plane (1 01) resulted in a reduction in the calculated crystallite size correspondingly. In addition, the (101) diffraction peak of the Cu-Zn/TiO_2 samples shifted to a higher angle (see Fig 2 (b)) implying the incorporation of copper effect in the TiO_2 lattice with the speculation that Ti^{4+} position may be replaced by copper due to their very small ionic radii difference (L´opez et al., 2009).

3.2. FTIR Study

The sample FTIR spectra in the 500-4000 cm^{-1} frequency range are shown in Fig. 3. The O-H peaks appeared due to the stretching and bending vibrations in the range 3200–3400 cm^{-1} and 1600 cm^{-1} respectively were well observed in the FTIR spectra (Chen et al., 2009; Venkatachalam et al., 2007).

Table 1. Lattice parameters and crystal size of un-doped TiO_2, 0.05, 0.10, 0.15 and 0.20 mmol Cu-Zn/TiO_2

Sample (mmol)	***Lattice Parameters***	***Cell Volume (A^3)***	***Crystallite size (nm)***
Un-doped TiO_2	a=b=3.78, c=9.48	135.45	18
0.05 Cu-Zn/TiO_2	a=b=3.79, c=9.51	136.60	16
0.10 Cu-Zn/TiO_2	a=b=3.78, c=9.52	136.02	15
0.15 Cu-Zn/TiO_2	a=b=3.80, c=9.53	137.61	13
0.20 Cu-Zn/TiO_2	a=b=3.80, c=9.48	136.89	18

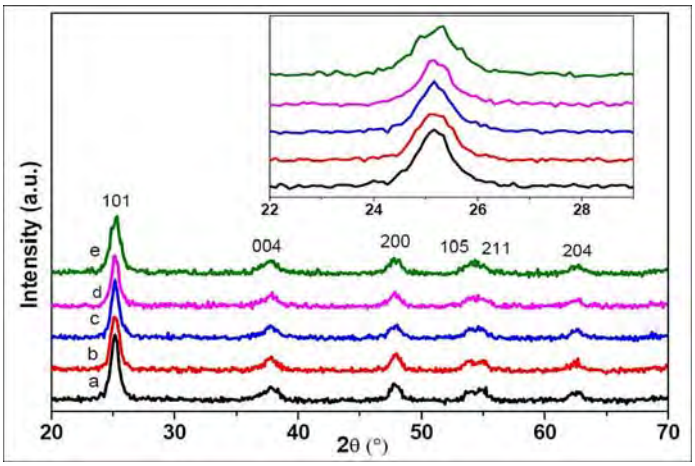

Fig. 2. XRD patterns of a-Un-doped TiO_2, b-0.05, c-0.10, d-0.15 and e-0.20 mmol of Cu-Zn-TiO_2 NPC. Inset is the enlarged XRD peaks of crystal plane (101)

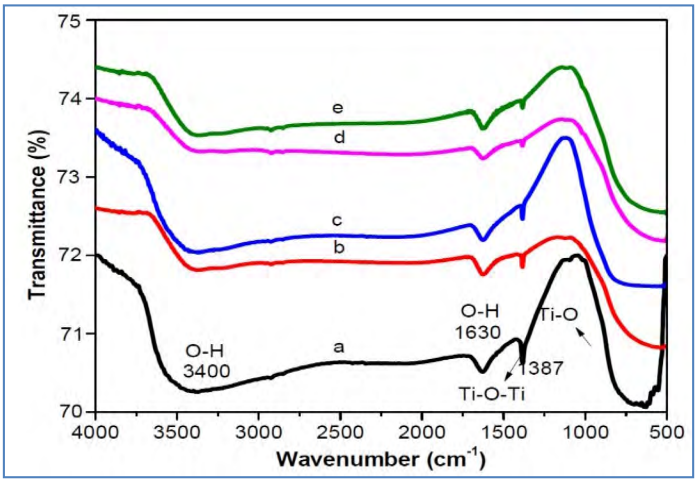

Fig. 3. FT-IR spectra of a-Un-doped TiO_2, b-0.05, c-0.10, d-0.15 and e-0.20 mmol of Cu^{2+}-Zn^{2+}/TiO_2 nanoparticles

The broad intense band in the range 450-700 cm^{-1} is due to the Ti-O stretching and Ti-O-Ti bridging stretching modes (Jagadale et al., 2008; Rao, 2019; Venkatachalam et al., 2007; Andra et al., 2016). The intensity of the peaks was greatly suppressed with an increase in the copper and zinc contents in the Cu-Zn-TiO_2 NPC compared to un-doped TiO_2. No extra peaks are present on Cu and Zn doping, promoting the effective dispersion of copper and Zinc, indicating the lack of copper and zinc clusters, which is a perfect agreement with the XRD assessment consequence.

3.3. FESEM Study

The surface structure and particle size were differentiated by FESEM. The sample surface morphology calcined at 400° C equal to a blend of nanoparticles is shown in Fig. 4. The electronic micrographs disclosed that the constituent particles appeared. The average particle size was about 20 nm.

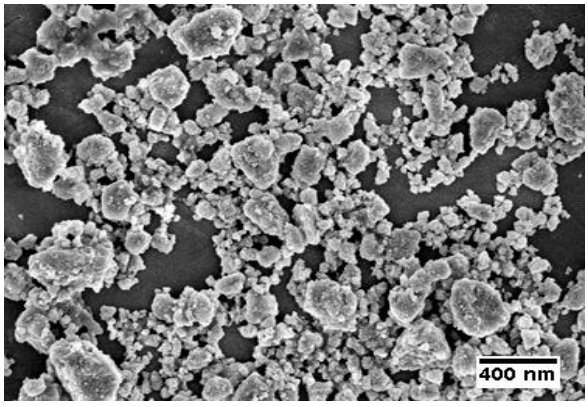

Fig. 4. FE-SEM images of 0.10 mmol Cu-Zn-TiO_2 NPC

3.4. EDX Study

The EDX spectra of Cu-Zn-TiO_2 NPC are shown in Fig. 5. Obviously, peaks associated with titanium, oxygen and the corresponding doped metal can be seen in this range. Results from an elemental assessment verified the homogeneous distribution of metal nanoparticles in the TiO_2 lattice.

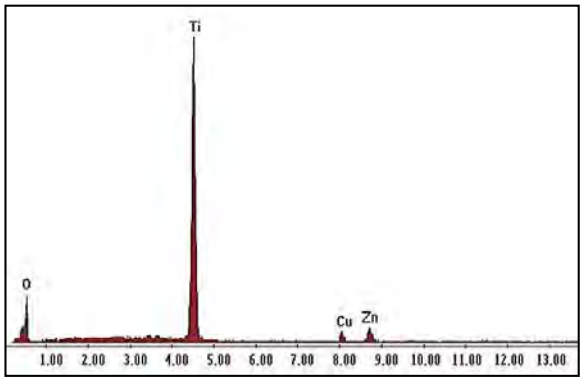

Fig. 5. EDX images of 0.1 mmol Cu-Zn-TiO_2 NPC

3.5. TEM and HR-TEM Study

TEM analysis was performed to investigate the average particle size and morphology.

It was noted that titania consisted almost solely of small-sized nanocrystallites. Most of the anatase TiO_2 material had a spherical morphology. The TEM images clearly revealed the spherical shaped nanoparticles in each sample (Fig. 6a for undoped TiO_2 and 6b for 0.15 mmol of copper and zinc co-doped TiO_2). The TiO_2 NPs being formed using copper and zinc and the TEM micrograph clearly illustrated the individual nanoparticles formed has the almost spherical shape 10-30 nm in size (Ma et al., 2004). When compared to the literature report (Ma et al., 2004), our experimental result supports the efficient synthesis of lesser size anatase TiO_2 nanoparticles. The sol-gel method found in copper and zinc is believed to have reduced titanium dioxide nanoparticles.

HR-TEM was used to clarify the surface planes for the TiO_2 particles. Fig. 6d shows the discrete apparent crystallites. The obviously spread edge of the anatase grid shows that the titania was extremely crystalline. HR-TEM found anatase nanocrystallites composed of tetragonal particles with (101) plane surfaces (Shklover et al., 1997).

Fig. 6e shows a processed image acquired by filtering technique after fast Fourier transformation of the TiO_2 particle. This technique analyzes the individual particles and demonstrates that the crystal composition was anatase with indexed (101) planes, which refers to the range in the anatase structure between the planes (101) (Patra et al., 2015, Takashi et al., 2011). Conclusively, the particle size of the calcined TiO_2 was reported that it was a pure single-phase anatase nanocrystalline material (Masuda and Kato, 2009).

The TEM images of undoped TiO_2 and 0.10 mmol of Cu-Zn/TiO_2 are shown in Figs. 6a and b. The particles in the TEM picture appeared to have different shapes and sizes. Agglomeration was obviously visible seen in the HR-TEM images (Fig. 6c, d). The average particle size observed about 20 nm.

3.6. Selected area electron diffraction

Fig. 7 (a) Indicates the crystallinity of titanium confirmed by the pattern of undoped TiO_2 chosen area electron diffraction (SAED) and (b) displays TiO_2 co-doped copper and zinc nanoparticles. The SAED model showed separate and good anatase-corresponding diffraction rings (Ma et al., 2004), demonstrating well-resolved bright and intense polymorphic ring patterns without any additional spots or second phase rings. Due to the lack of an amorphous nature it disclosed the typical diffraction rings for a crystalline powder. Analysis of TEM micrograph image processing is a helpful way to fine-tune the microstructure.

It can be indexed to reflect tetragonal structure in crystallography, and this outcome has also been studied through X-ray diffraction. Tropism of the particles at random and tiny particles leads diffraction rings to widen, which consists of many diffraction places, indicating that the nanoparticles are polycrystalline structures. Electron diffraction indicates that each particle consists of many tiny crystal nuclei, compelling evidence that the particles grow in a model of aggregation. The copper and zinc co-doped TiO_2 NPs chosen area electron diffraction (SAED) micrograph (Fig. 7b) demonstrates the tetragonal crystalline structure with indexed diffracting planes.

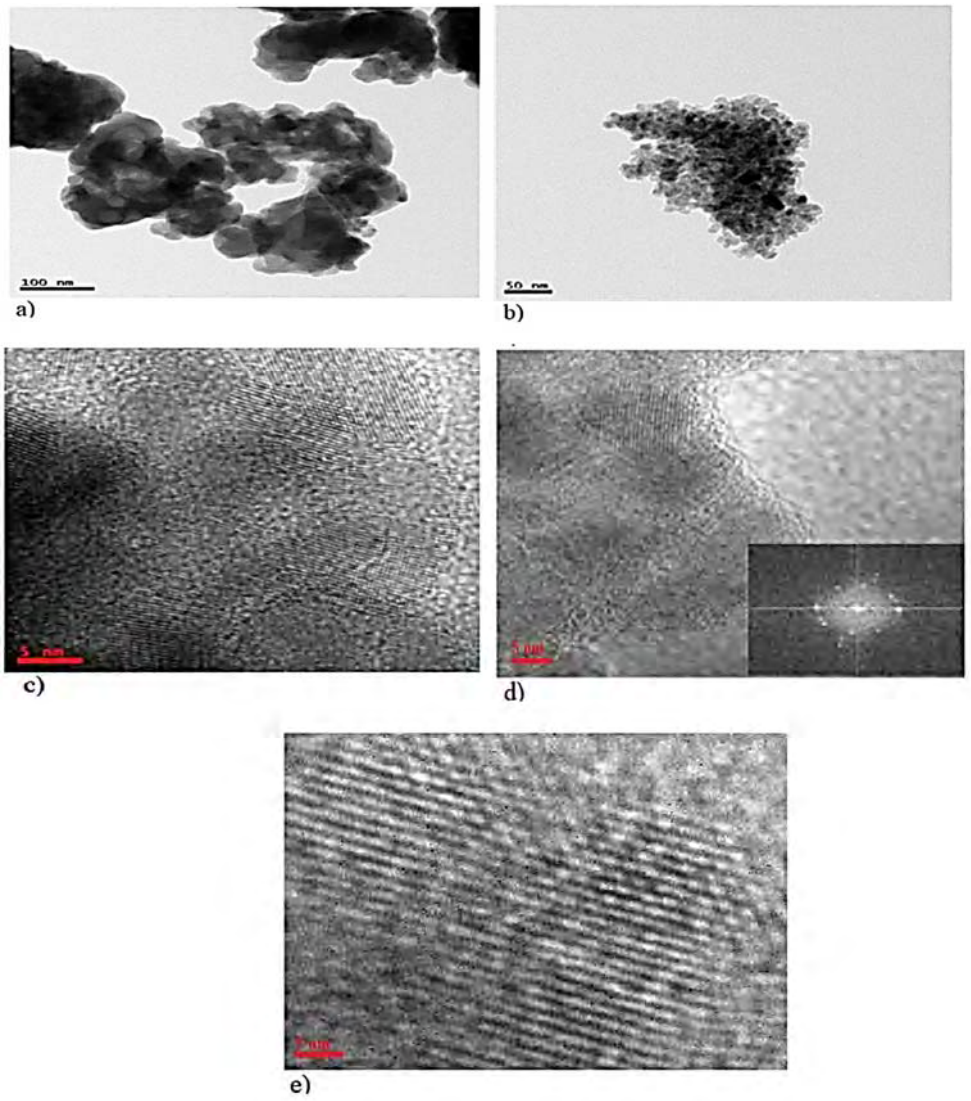

Fig. 6. TEM images of: a) Undoped TiO_2, b) 0.15 mmol of Cu-Zn-TiO_2 NPC, c) and d) HRTEM images of Undoped TiO_2 and Cu-Zn-TiO_2 NPC nanoparticles e) Filtered lattice image of HR-TEM image

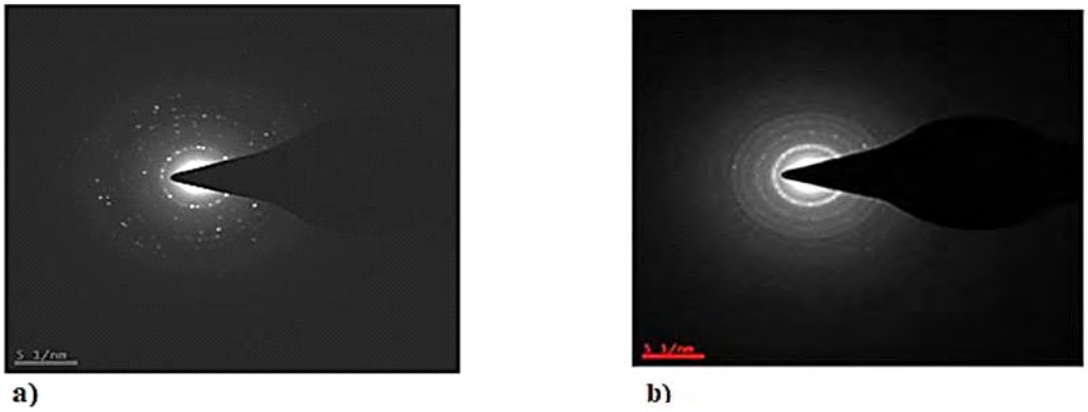

Fig. 7. SAED images of: a) Undoped TiO_2 and b) 0.15 mmol of Cu^{2+}-Zn^{2+}/TiO_2 nanoparticles

3.7. UV-Visible Diffusion Reflectance Spectroscopy

The UV-visible absorption spectra of un-doped TiO_2 and 0.05, 0.10, 0.15 and 0.20 mmol of Cu^{2+}-Zn^{2+}/TiO_2 and are shown in Fig. 8. The edge of the UV-vis absorption band is a strong function of titania nano clusters. (Li et al., 2004; Anpo et al., 1987). Fig. 8. shows the UV-vis absorption spectrum of un-doped TiO_2 and Cu-Zn/TiO_2.

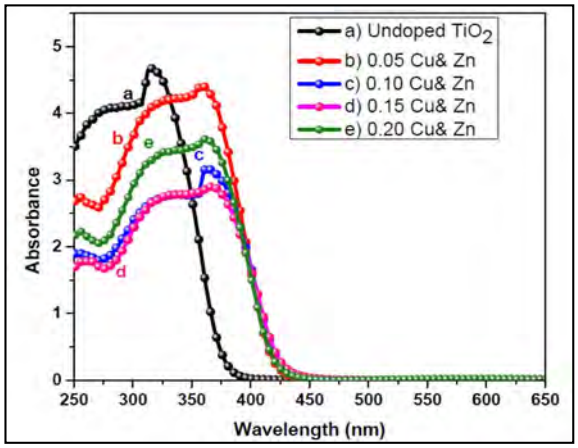

Fig. 8. UV-Visible absorption spectra of (a) undoped TiO_2, (b) 0.05 (c) 0.10 (d) 0.15 and (e) 0.20 mmol of Cu^{2+}-Zn^{2+}/TiO_2 nanoparticles

In addition, undoped TiO_2 shows almost no slight absorption capacity in the visible region (>400 nm), while Zn, Cu co-doped TiO_2 samples show a red shift of the absorption edge and a significant increase in light absorption at 400-600 nm. It is known that doping with some metal elements can modify the band gap of TiO_2. The reason is that transition metal ions (Cu^{2+}/Cu^{+}, Cu^{+}/Cu^{0}, or Zn^{2+}/Zn^{0}) can introduce new energy levels into the TiO_2 band gap. Consequently, the absorption edges of the co-doped TiO_2 sample from the dopant energy level electronic transformation (Zn^{2+}/Zn^{0} or Cu^{2+}/Cu^{+}, Cu^{+}/Cu^{0}) to TiO_2 conductive band should shift towards longer wave lengths for the Zn, Cu. In view of these, the increased absorption in the visible region can be attributed to the excitation of Zn^{2+} or Cu^{2+} 3D electrons to the TiO_2 conductive band (charge transfer transition) resulting in a 350 nm centered band. In addition, the absorption intensity presents at 400-600 nm, Could be assigned to the d-d transition of Zn^{2+} ($2T_{2g} \rightarrow 2A_{2g}$, $2T_{1g}$) or the charger transfer transition between the copper ions ($Cu^{+}+Cu^{+} \rightarrow Cu^{2+}+Cu^{0}$) that interact. In conclusion, the increase in UV-Visible absorption increases the number of photogenerated electrons and holes employed in the photocatalytic process, which can increase the quantity output and therefore the photocatalytic activity of TiO2 (Lettmann et al., 2001). Once it has been reported that there is a strong correlation between light absorption characteristics and photocatalytic activity, it is a great way to achieve elevated visible photocatalytic activity by enhancing the photocatalytic absorption capacity. This shift of the absorption edge to longer wavelengths for Cu^{2+}-Zn^{2+}/TiO_2 shows the presence of excellent interaction between TiO_2 and Cu^{2+}, Zn^{2+} seeds and improves the photocatalytic activity of catalysts in visible light. This band confirms the presence of TiO_2's anatase crystal shape (Venkatachalam et al., 2007). TiO_2 is well known to be semiconductor with a 3.0-3.2 eV band gap. After an energy level of impurity is introduced, the edge of absorption will change to the region of visible light. This leads the final product to change color. Since separate dopants give different levels of impurity energy, doped TiO_2 of separate colors is achieved.

3.8. Adsorption study of the catalyst

The amount of catalyst needed for decontamination has been optimized as 0.1 g L^{-1} for degradation of bispyribac sodium, any further increase of catalyst had no significant effect on degradation. The adsorption of catalyst study was conducted by quantifying the concentration of bispyribac sodium in water for a period of three hours. The recovery was 90 to 96%, 91 to 95%, 91 to 96% in acidic water, neutral water and basic water respectively. The results indicate no significant loss of residues due to adsorption. In the presence of the catalyst though, the dissipation was found rapid under sunlight.

3.9. LOQ Determination

The LOQ was evaluated to be 0.02 mg/L. This quantification limit represents the spiked level at which an analyte peak was continuously produced roughly 10 times the baseline noise in the chromatogram.

3.10. Photolytic and photocatalytic study

The photolytic degradation results of bispyribac sodium in water showed the residues are highly stable, the stability decreased with decreasing pH. The results were shown in Table 2. Comparatively lower values of bispyribac sodium in the presence of a catalyst (Photocatalytic) in different pH were recorded. The results were shown in Table 3.

The dissipation curve was plotted between the sampling occasions and a concentration of the analyte is shown in Fig. 9 and Fig 10. The DT50 (time required to degrade 50% of residues i.e. half-life) value was calculated using the following formula (Nageswara Rao et al., 2016, Rao, 2019) (Eq. 1):

$$DT50 = \ln(2)/k \qquad (1)$$

Where '*K*' is the slope of the curve occurred from the dissipation data. The rate constant has been determined by the linear regression equation exploiting the first order rate equation (Eq. 2):

$$K = \ln(a/(a-b))/dt \qquad (2)$$

Table 2. Photolysis of bispyribac-sodium under direct sunlight in different pH waters

Occasion (Days)	*Test dose (bispyribac-sodium @0.1 mg/L)*		
	Acidic water	*Neutral water*	*Basic water*
0	0.100	0.099	0.1
5	0.082	0.092	0.097
10	0.051	0.084	0.092
30	0.024	0.071	0.085
50	<LOQ	0.058	0.078
100		0.021	0.063
150		<LOQ	0.036
200			<LOQ

Table 3. Photocatalysis of bispyribac-sodium in different pH waters

Occasion (Hours)	*Test dose (bispyribac-sodium @0.1 mg/L)*		
	Acidic water	*Neutral water*	*Basic water*
0	0.099	0.099	0.1
6	0.067	0.092	0.091
12	0.052	0.081	0.080
24	0.037	0.067	0.072
36	0.022	0.052	0.063
72	<LOQ	0.021	0.044
120		<LOQ	<LOQ

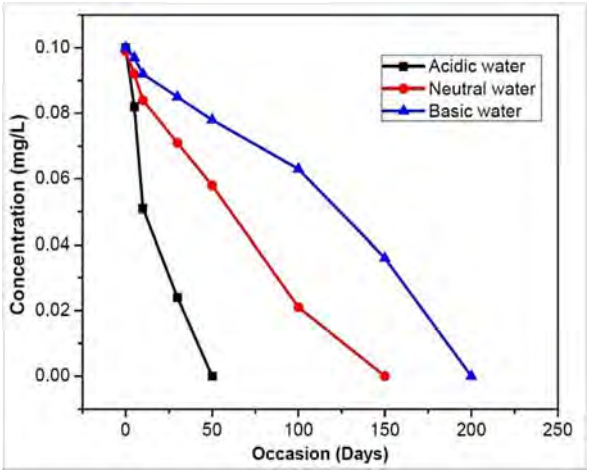

Fig. 9. Photolytic dissipation curve of bispyribac sodium in different pH waters

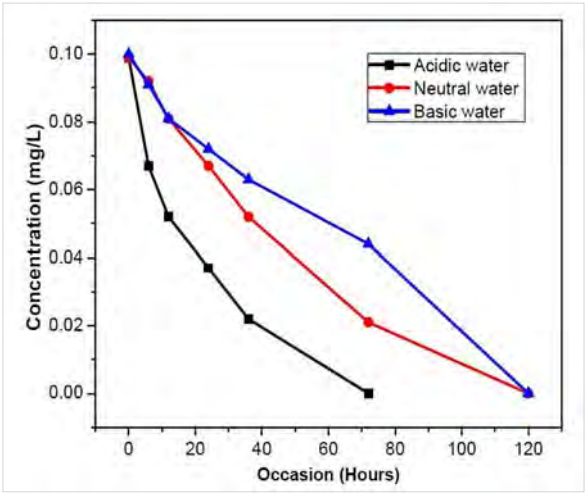

Fig. 10. Photocatalytic dissipation curve of bispyribac sodium in different pH waters

The DT50 of bispyribac-sodium evaluated by regression analysis of the dissipation data. The calculated DT 50 values are presented in Table 4. It shows variation with different water samples (acidic, neutral and basic).

Table 4. DT 50 values of bispyribac sodium in different pH waters

DT 50 (Half-life)			
Degradation	***pH-4***	***pH-7***	***pH-9***
Photolytic (Days)	14.57	46.35	111.03
Photocatalytic (Hours)	17.60	31.98	62.52

3.11. Effect of surfactants

To study the effects of surfactants on pesticide decontamination in water, experiments were carried out by adding 10^{-2} mole/L concentrations of cationic surfactants CTAB, anionic surfactant SDS and nonionic surfactant Brij-35. It was observed that there was no effect on photocatalytic decontamination of bispyribac sodium.The summarized results for effect of surfactants amount are presented in Table 5 and Fig. 11. The dissipation details of bispyribac sodium with effect of surfactants and catalyst results were shown in Table 6.

Table 5. Dissipation data for effect of surfactant on of bispyribac sodium in water

Occasion (hours)	*Residues (µg/mL)*		
	CTAB	*SDS*	*Brij-35*
0	0.098	0.1	0.099
6	0.091	0.093	0.090
12	0.082	0.083	0.079
24	0.064	0.067	0.061
36	0.054	0.051	0.057
72	0.031	0.034	0.029
120	<LOQ	<LOQ	<LOQ

Table 6. DT 50 (Half-life) values of bispyribac sodium with influenced surfactants and catalyst

DT 50 (Half-life)			
Degradation	CTAB	SDS	Brij-35
Photocatalytic (Hours)	42.77	44.82	41.27

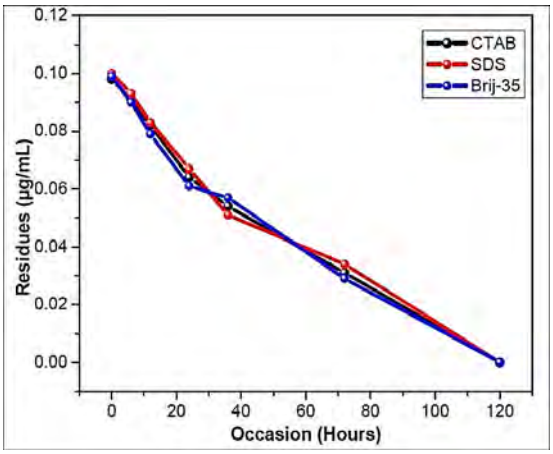

Fig. 11. Dissipation curve of bispyribac sodium influenced surfactants and catalyst

3.12. Effect of humic acid content on pesticide degradation

To determine the effective content of humic acid for rapid degradation of pesticide in water on the photocatalytic decontamination, Experiments were conducted to vary the quantity of humic acid in water from 0 to 20 mg/L. No increase in the rate of bispyribac sodium was observed from the experimental results.The summarized results for effect of humic acid are presented in Table 7 and Fig. 12. The dissipation details of bispyribac sodium with effect of humic acid and catalyst results were shown in Table 8.

Table 7. Dissipation data for effect of humic acid on decontamination of bispyribac sodium in water

	Residues (µg/mL)		
Occasion (hours)	***0 mg/L Humic acid content***	***10 mg/L Humic acid content***	***20 mg/L Humic acid content***
0	0.099	0.098	0.096
6	0.090	0.084	0.0075
12	0.079	0.071	0.063
24	0.062	0.057	0.052
36	0.051	0.052	0.047
72	0.029	0.027	0.025
120	<LOQ	<LOQ	<LOQ

Table 8. DT 50 (Half-life) values of bispyribac sodium with influenced humic acid and catalyst

DT 50 (Half-life)			
Humic acid content	0 mg/L	10 mg/L	20 mg/L
Photocatalytic (Hours)	40.41	40.34	40.06

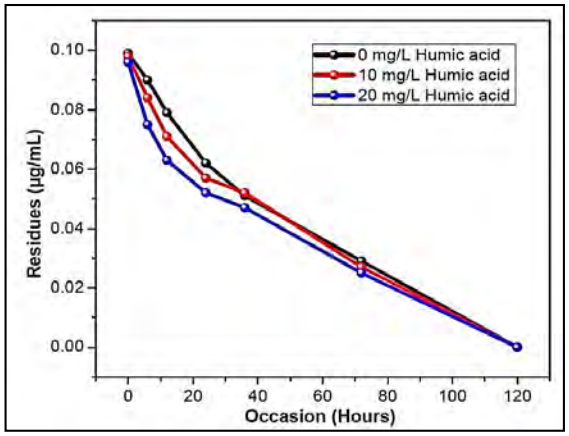

Fig. 12. Dissipation curve of bispyribac sodium influenced with surfactants humic acid and catalyst

3.13. Confirmation of residues by electrospray mass spectrometry (LC-ESI-MS/MS)

The presence of residues in water samples was confirmed by analysing representative samples using high capacity ion trap LC-ESI-MS/MS. The parent compound bispyribac sodium eluted at 5.3 min and obtained a peak of molecular ions at m/Z 453 and the fragment ions appeared at 435 and 297. The total ion chromatogram for the residues in standard, on 12th-hour photocatalytic water LCMS/MS spectra were shown in Fig. 13.

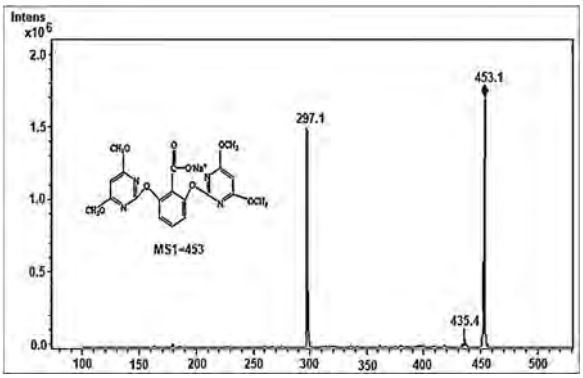

Fig. 13. LCMS/MS of bispyribac sodium in 12th-hour sample

4. Conclusions

In the present study, Cu-Zn-TiO_2 NPC was synthesized through a sol-gel process and characterization has been carried out by using XRD, Uv-DRS, FT-IR, FE-SEM, EDS and HR-TEM. It was found from the data that doping of TiO_2 with Cu-Zn reduces the size of the particle, decrease in crystallite size and band gap, which ultimately leads to the efficiency of photocatalytic activity.

Photocatalytic studies of bispyribac sodium at various conditions such as acidic, basic and neutral reveals that the activity is enormously increased with co-doped TiO_2 as the time frame is fixed for a stipulated number of hours. It can, therefore, be claimed that the newly synthesized co-doped TiO_2 is

proven to be effective for bispyribac sodium photocatalysis. The decontamination effect of Cu-Zn-TiO_2 NPC under laboratory conditions in water indicated that lower pH is more favorable for faster degradation under sunlight.

References

Amoros-Perez A., Cano-Casanova L., Castillo-Deltell A., Román-Martínez A., Carmen M., (2019), TiO_2 modification with transition metallic species (Cr, Co, Ni, and Cu) for photocatalytic abatement of acetic acid in liquid phase and propene in gas phase, *Materials*, **12**, 1-18.

Andra P., Ekaterina M., Andrei P., Andrei B., Mirela S., Cristian P., (2016), Removal of hexavalent chromium from waters by means of a TIO_2-Fe_3O_4 nanocomposite, *Environmental Engineering and Management Journal*, **15**, 989-994.

Anpo M., Shima T., Kodama S., Kobokawa Y., (1987), Photocatalytic hydrogenation of propyne with water on small-particle titania: size quantization effects and reaction intermediates, *The Journal of Physical Chemistry*, **91**, 4305-4310.

Asahi R., Morikawa T., Ohwaki. T., Aoki K., Taga Y., (2001), Visible-light photocatalysis in nitrogen-doped titanium oxides, *Science*, **293**, 269-271.

Byrne C., Moran L., Hermosilla D., Merayo N., Blanco A., Rhatigan S., Hinder S., Ganguly P Nolan M., Pillai S.C., (2019), Effect of Cu doping on the anatase-to-rutile phase transition in TiO_2 photocatalysts: Theory and experiments, *Applied Catalysis B: Environmental*, **246**, 266-276.

Cao Y., Yang Y., Zhang W.S., Liu W.F., Yue P., (2004), Improved the photocatalytic activity of Sn^{4+} doped TiO_2 nanoparticulate films prepared by plasma-enhanced chemical vapor deposition, *New Journal of Chemistry*, **28**, 218-222.

Chen X., Wang X., Fu X., (2009), Hierarchical macro/mesoporous TiO_2/SiO_2 and TiO_2/ZrO_2 nanocomposites for environmental photocatalysis, *Energy and Environmental Science*, **2**, 872-877.

Choi W. Termin A., Hoffmann M.R., (1994), The Role of metal ion dopants in quantum-sized TiO_2: Correlation between photoreactivity and charge carrier recombination dynamics, *Journal of Physical Chemistry*, **98**, 13669-13679.

Dawson A., Kamat P.V., (2001), Semiconductor metal nanocomposites. Photoinduced fusion and photocatalysis of gold-capped TiO_2 (TiO_2/Gold) Nanoparticles, *Journal of Physical Chemistry B*, **105**, 960-966.

Fujishima A., Rao. T.N., Tryk. D.A., (2000), Titanium dioxide photocatalysis, *Journal of Photochemistry and Photobiology C: Photochemistry Reviews*, **1**, 1-21.

Gao B.F., Ma Y., Cao Y.A., Yang W.S., Yao J.N., (2006), Great enhancement of photocatalytic activity of nitrogen-doped titania by coupling with tungsten oxide, *Journal of Physical Chemistry B*, **110**, 14391-14397.

Ge L., Xu M., Sun M., Fang H., (2006), Low-temperature synthesis of photocatalytic TiO_2 thin film from aqueous anatase precursor sols, *Journal of Sol-Gel Science and Technology*, **38**, 47-53.

Geraldine L., Leonard, M., Carlos A., Paez, Alfonso E., Ram´ırez, Julien G., Benoıt H., (2018), Interactions between Zn^{2+} or ZnO with TiO_2 to produce an efficient photocatalytic, superhydrophilic and aesthetic glass, *Journal of Photochemistry and Photobiology A: Chemistry*, **350**, 32-43.

Impellizzeri G., Scuderi V., Romano L., Sberna P.M., Arcadipane E., Sanz R., Scuderi M., Nicotra G., (2016), Fe ion-implanted TiO_2 thin film for efficient visible-light photocatalysis Fe ion-implanted TiO_2 thin film for efficient visible-light photocatalysis, *Journal of Applied Physics*, **116**, 173507-1-173507-8.

Jagadale T.C., Takale S.P., Sonawane R.S., Joshi H.M., Patil S.I., Kale B.B., Ogale. S.B., (2008), N-Doped TiO_2 nanoparticle-based visible light photocatalyst by modified peroxide sol-gel method, *Journal of Physical Chemistry C*, **112**, 14595-14602.

Kim S., Choi W., (2005), Visible-light-induced photocatalytic degradation of 4-chlorophenol and phenolic compounds in aqueous suspension of pure titania: demonstrating the existence of a surface-complex-mediated path, *Journal of Physical Chemistry B*, **109**, 5143-5149.

Lettmann C., Hildenbrand K., Kisch H., Macyk W., Maier W.F., (2001), Visible light photodegradation of 4-chlorophenol with a coke-containing titanium dioxide photocatalyst, *Applied Catalysis B: Environmental*, **32**, 215-227.

Li X.Z., Li F.B., (2001), Study of Au/Au^{3+}-TiO_2 photocatalysts toward visible photooxidation for water and wastewater treatment, *Environmental Science and Technology*, **35**, 2381-2387.

Li W., Wang Y., Lin H, Shah S.I., Huang C.P., Doren D.J., Rykov S.A., Chen J.G., Barteau M.A., (2003), Band gap tailoring of Nd^{3-} doped TiO_2 nanoparticles, *Applied Physics Letters*, **83**, 4143-4145.

Li Y., White T.J., Kim S.H.J., (2004), Low-temperature synthesis and microstructural control of titania nanoparticles, *Journal of Solid State Chemistry*, **177**, 1372-1381.

L´opez R., G´omez R., Llanos M.E., (2009), Photophysical and photocatalytic properties of nanosized copper-doped titania sol-gel catalysts, *Catalysis Today*, **148**, 103-108.

Mohamed M.A., Jaafar J., Zain M.F.M., Minggu L.J., Kassim M.B.,., Rosmi M.S., Alias N.H., Nor N.A.M., Salleh W.N.W., Othman M.H.D., (2018), In-depth understanding of core-shell nanoarchitecture evolution of g-C3N4@C, N co-doped anatase/rutile: Efficient charge separation and enhanced visible-light photocatalytic performance, *Applied Surface Science*, **436**, 302-318.

Ma R., Sasaki T., Bando Y.J., (2004), Layer-by-layer assembled multilayer films of titanate nanotubes, Ag- or Au-loaded nanotubes, and nanotubes/nanosheets with polycations, *Journal of the American Chemical Society*, **126**, 10382-10388.

Mahy J.G., Cerfontaine V., Poelman D., Devred F., Gaigneaux E.M., Heinrichs B., Stephanie D.L., (2018), Highly efficient low-temperature N-doped TiO_2 catalysts for visible light photocatalytic applications, *Materials*, **11**, 2-20.

Masuda Y., Kato K., (2009) Synthesis and phase transformation of TiO_2 nano-crystal in aqueous solutions, *Journal of the Ceramic Society of Japan*, **117**, 373-376.

Moon J., Yun C.Y., Chung K.W., Kang M.S., Yi J., (2003), Photocatalytic activation of TiO_2 under visible light using Acid Red 44, *Catalysis Today*, **87**, 77-86.

Nageswara Rao T., Apparao K., Murthy S.N.V.S., Manohara Naidu T., (2016), Applications of zinc oxide nanoparticles as catalyst in dissipation kinetics of

s-metolachlor herbicide in different pH waters under direct sun light, *Materials Today: Proceedings*, **3**, 3799-3804.

Patra S., Davoisne C., Bouyanfif H., (2015), Phase stability frustration on ultrananosized anatase TiO_2, *Scientific Reports*, **5**, 10928, https://doi.org/10.1038/srep10928

Pelaez M., Nolan N.T., Pillai S.C., Seery M.K., Falaras P., Kontos A.G., Dunlop P.S.M., Hamilton J.W.J., Byrne J.A., O'Shea K., Entezari M.H., Dionysiou D.D., (2012), A review on the visible light active titanium dioxide photocatalysts for environmental applications, *Applied Catalysis B: Environmental*, **125**, 331-349.

Rao T.N., (2019), Photo catalytic applications of $FeTiO_2$ nanoparticles in dissipation kinetics of herbicide residues in soils, *Research Journal of Biotechnology*, **14**, 54-63.

Rehman S., Ullah R., Butt A.M., Gohar N.D., (2009), Strategies of making TiO_2 and ZnO visible light active, *Journal of Hazardous Materials*, **170**, 560-569.

Shklover V., Nazeeruddin M.K., Zakeeruddin S.M., Barbe C., Kay A., Haibach T., Steurer W., Hermann R., Nissen H.-U., Gratzel M., (1997), Structure of nanocrystalline TiO_2 powders and precursor to their highly efficient photosensitizer, *Chemistry of Materials*, **9**, 430.

Takashi T., Yamashita S., Majima T., (2011), Evidence for crystal-face-dependent TiO_2 Photocatalysis from single-molecule imaging and kinetic analysis, *Journal of the American Chemical Society*, **133**, 7197-7204.

Tobaldia D.M., Piccirillo C., Rozman N., Pullara R.C., Seabraa M.P., Sever A., Castro P.M.L., Labrinch J.A (2016), Effects of Cu, Zn and Cu-Zn addition on the microstructure and antibacterial and photocatalytic functional properties of Cu-Zn modified TiO_2 nano-hetero structures, *Journal of Photochemistry and Photobiology A: Chemistry*, **330**, 44-54.

Venkatachalam N., Palanichamy M., Arabindoo B., Murugesan V., (2007), Enhanced photocatalytic degradation of 4-chlorophenol by Zr^{4+} doped nano TiO_2, *Journal of Molecular Catalysis A: Chemical*, **266**, 158-165.

Zhang L., Guo J., Yan T., Han Y., (2018), Fibroblast responses and antibacterial activity of Cu and Zn co doped TiO_2 for percutaneous implants, *Applied Surface Science*, **434**, 633-642.